



Lu, X.Z., Chen, J.F., Ye, L.P., Teng, J.G. and Rotter, J.M. (2005) "Theoretical analysis of FRP stress distribution in u jacketed RC beams", *Proc. 3rd Int. Conference on Composites in Construction (CCC2005)*, July, Lyon, France, 541-548.

THEORETICAL ANALYSIS OF FRP STRESS DISTRIBUTION IN U JACKETED RC BEAMS

X.Z. Lu¹, J.F. Chen², L.P. Ye¹, J.G. Teng³ and J.M. Rotter²

¹ Department of Civil Engineering, Tsinghua University, Beijing, China

² Institute for Infrastructure and Environment, Edinburgh University
The King's Buildings, Edinburgh EH9 3JN, UK

³ Department of Civil and Structural Engineering, The Hong Kong Polytechnic University
Hong Kong, China

ABSTRACT: Reinforced concrete (RC) beams may be strengthened for shear with externally bonded fibre reinforced polymer (FRP) composites through one of three common schemes: complete wrapping, U jacketing, and bonding on their sides only. The two main shear failure modes in such strengthened beams are FRP rupture and FRP debonding. In both failure modes, the stress (or strain) distribution in the FRP at the ultimate state is non-uniform and is a key factor influencing the contribution of the FRP to the shear capacity of the beam. This paper presents a theoretical study on the stress distribution in the FRP along the critical shear crack at debonding failure of U jacketed beams for several assumed crack width variations using a rigorous FRP-to-concrete bond-slip model. Numerical results show that Chen and Teng's [1, 2] simple assumption of stress distributions in the FRP results in satisfactory predictions of the shear strength.

1. INTRODUCTION

Extensive research has been conducted on the strengthening of reinforced concrete (RC) beams with externally bonded fibre reinforced polymer (FRP) composites [1-16]. RC beams can be strengthened through complete wrapping, U jacketing or bonding on their sides only. The main shear failure modes in shear-strengthened beams are FRP rupture and FRP debonding [14, 15]. In both failure modes, the stress (or strain) distribution in the FRP at the ultimate state is non-uniform and a key factor influencing the contribution of the FRP to the shear capacity of the beam for all three strengthening schemes mentioned above [2, 16]. Based on a number of simple but rational assumptions, Chen and Teng [2,16] proposed methods for predicting the maximum values of the FRP stress and the stress distribution factors at the ultimate limit state for both failure modes.

Among the above three strengthening schemes, U jacketing is probably the most commonly used in practice. Complete wrapping, although most effective, is often difficult to implement in application (e.g. difficult to apply to T beams unless holes are cut through the flange), whilst side bonding is the least effective [13]. Both FRP rupture and FRP debonding can occur in U jacketed beams. This paper presents a simple theoretical study on the stress distribution in the FRP along the critical shear crack at debonding failure in U jacketed beams. A recently developed FRP-to-concrete bond-slip model [17] is used in the analysis. Several idealised crack width variations, which are closely related to the FRP slip field due to the critical shear crack, are investigated. The results are compared with Chen and Teng's [2] simple predictive model. For convenience of description, the bonded FRP reinforcement is assumed to be in the form of strips, with a continuous sheet being a special case or a smeared equivalent representation of strips. Depending on the context, either strips or sheets may be used to refer to the bonded FRP reinforcement.

2. EXISTING SHEAR STRENGTH MODELS FOR FRP DEBONDING

A number of models for the shear strength of FRP-strengthened RC beams have been proposed for design use [2, 5, 9, 11, 12, 16]. In most of these proposals, the shear strength of an FRP-strengthened RC beam V_n is evaluated by assuming that the contributions of the concrete V_c , the steel shear reinforcement V_s and the bonded FRP reinforcement V_f are additive, i.e.

$$V_n = V_c + V_s + V_f \quad (1)$$

Because it is usually proposed that V_c and V_s should be calculated according to provisions in existing design codes, the main differences between the available proposals lie in the evaluation of the FRP contribution V_f .

Steel stirrups have a small elastic strain limit but excellent ductility, so all stirrups intersected by the critical shear crack can reach their yield stress at the shear failure of the RC beam as a result of stress re-distribution. This means that their yield strength is fully utilized and the stress distribution in the steel stirrups along the intersecting critical shear crack is uniform. By contrast, both FRP rupture and FRP debonding are brittle processes that allow little or limited stress redistribution, so the stress distribution in the FRP along the shear crack at the ultimate state is non-uniform and can significantly affect the FRP contribution to the shear capacity of the beam.

Chen and Teng [1, 15] were probably the first to propose the explicit inclusion of the effect of non-uniform stress distribution in the FRP on the shear capacity. The FRP contribution in their model [2, 16] is given by:

$$V_f = 2f_{fe}t_f w_f \frac{h_{fe}(\cot \theta + \cot \beta) \sin \beta}{s_f} \quad (2)$$

where θ is the critical shear crack angle, h_{fe} is the effective height of the FRP, w_f is the width of the FRP strip, s_f is the centre to centre spacing of FRP strips along the beam longitudinal axis, and the effective FRP stress f_{fe} is defined as the maximum FRP stress $\sigma_{f,max}$ times the stress distribution factor D_f

$$f_{fe} = D_f \sigma_{f,max} \quad (3)$$

For debonding failures, the maximum FRP stress $\sigma_{f,max}$ is calculated according to Chen and Teng's bond strength model [18], which is given as:

$$\sigma_{f,max} = \min \left\{ \begin{array}{l} f_{fu} \\ 0.427 \beta_L \beta_w \sqrt{\frac{E_f \sqrt{f'_c}}{t_f}} \end{array} \right., \quad \beta_L = \begin{cases} 1 & \text{if } \lambda \geq 1 \\ \sin \frac{\pi \lambda}{2} & \text{if } \lambda < 1 \end{cases}, \quad \lambda = \frac{L_{max}}{L_e} \quad (4a,b,c)$$

$$L_{max} = \begin{cases} \frac{h_{fe}}{\sin \beta} & \text{for U-jackets} \\ \frac{h_{fe}}{2 \sin \beta} & \text{for side plates} \end{cases}, \quad L_e = \sqrt{\frac{E_f t_f}{\sqrt{f'_c}}}, \quad \beta_w = \sqrt{\frac{2 - w_f / (s_f \sin \beta)}{1 + w_f / (s_f \sin \beta)}} \quad (4d,e,f)$$

Assuming that all bonded FRP strips intersected by the critical shear crack can develop the full bond strength at the ultimate limit state, Chen and Teng [1, 2] deduced the FRP stress distribution factor as

$$D_f = \begin{cases} \frac{2}{\pi\lambda} \frac{1 - \cos \frac{\pi\lambda}{2}}{2} & \text{if } \lambda \leq 1 \\ 1 - \frac{\pi - 2}{\pi\lambda} & \text{if } \lambda > 1 \end{cases} \quad (5)$$

Because both D_f and β_L are functions of the normalised maximum bond length λ , the following modified FRP stress factor D_{FL} is defined here for convenience of comparison with numerical results presented later:

$$D_{fL} = D_f \beta_L \quad (6)$$

Using Eq. 6, the effective FRP stress of Eq. 3 can alternatively be expressed as:

$$f_{fe} = D_f \sigma_{f \max} = D_f \beta_L \sigma_{f, \inf} = D_{fL} \sigma_{f, \inf} \quad (7)$$

where $\sigma_{f, \inf}$ is the FRP debonding stress when the FRP bond length is infinite:

$$\sigma_{f, \inf} = 0.427 \beta_w \sqrt{\frac{E_f \sqrt{f_c'}}{t_f}} \quad (8)$$

Furthermore, for ease of comparison for different forms of crack width variations and for both U jacketing and side bonding, a normalised bond length at the middle of the critical shear crack λ' is defined here, which can be related to the normalised maximum bond length λ for U jacketing as follows:

$$\lambda' = \frac{L_{mid}}{L_e} = \frac{h_{fe}}{2L_e \sin \beta} = \frac{\lambda}{2} \quad (9)$$

Clearly, the assumption adopted by Chen and Teng [2] for deriving the FRP stress distribution factor that all FRP strips intersected by the critical shear crack can reach the full bond strength at the ultimate limit state is simplistic. The aim of this study is to assess the validity of this assumption.

3. IDEALISATION OF FRP SLIP FIELD ALONG CRITICAL SHEAR CRACK

Shear cracking in concrete beams is a complex phenomenon and there is still a lack of accurate methods for predicting the initiation and propagation of these cracks. Depending on many factors such as loading, amount and detailed arrangement of internal reinforcement and the properties of concrete, there may be one or more diagonal cracks. However, unless the shear failure is due to diagonal compression which often occurs in beams with very small shear span-to-depth ratios, there is usually a critical shear crack which dominates the shear failure process. In some beams, such as those with large shear span-to-depth ratios, the critical shear crack may be the only crack intersecting the FRP strips on the beam sides. It may be noted that the FRP-to-concrete bond strength is increased if there are more than one crack intersecting the FRP strip [19]. Therefore, it is conservatively assumed in this study that secondary shear cracks are insignificant compared with the critical shear crack intersecting the FRP strips in determining the interfacial behaviour between the FRP strip and the concrete substrate.

Provided that the critical shear crack is predominant over other shear cracks, the interfacial slips (and thus stresses) between an FRP strip and the substrate concrete is then almost wholly induced by the widening of this crack. Clearly, the sum of the interfacial slips on both sides of the critical shear crack is equal to the crack width. This means that the bond slip behaviour of the FRP-to-concrete interface is predominately controlled by the width of the critical shear crack at the location where it intersects the FRP strip, and that the variation of this width determines the stress distribution in the FRP along the critical shear crack.

Because of the lack of information on the precise shape of the critical shear crack, four simple crack types as shown in Fig. 1 are considered in this study. Note that the shape of the critical shear crack may be close to Type A (Fig. 1a) in beams very heavily reinforced in flexure, whilst it is expected to be closer to Type C (Fig. 1c) in beams with minimal flexural reinforcement. The crack shape for most practical beams is likely to lie between these two cases and may be close to Type B (Fig. 1b). If the FRP strips cover only part of the beam height, it is possible that the critical shear crack is fairly uniform within the effective FRP height (Fig. 1d). If it is further assumed that the slips between FRP and concrete on the two sides of the critical shear crack are symmetrical, which means that the distribution of slip along the critical shear crack is assumed to follow the shape of the crack. The FRP slip fields corresponding to the four crack shapes are termed here as Slip Fields A – D respectively (Fig. 1).

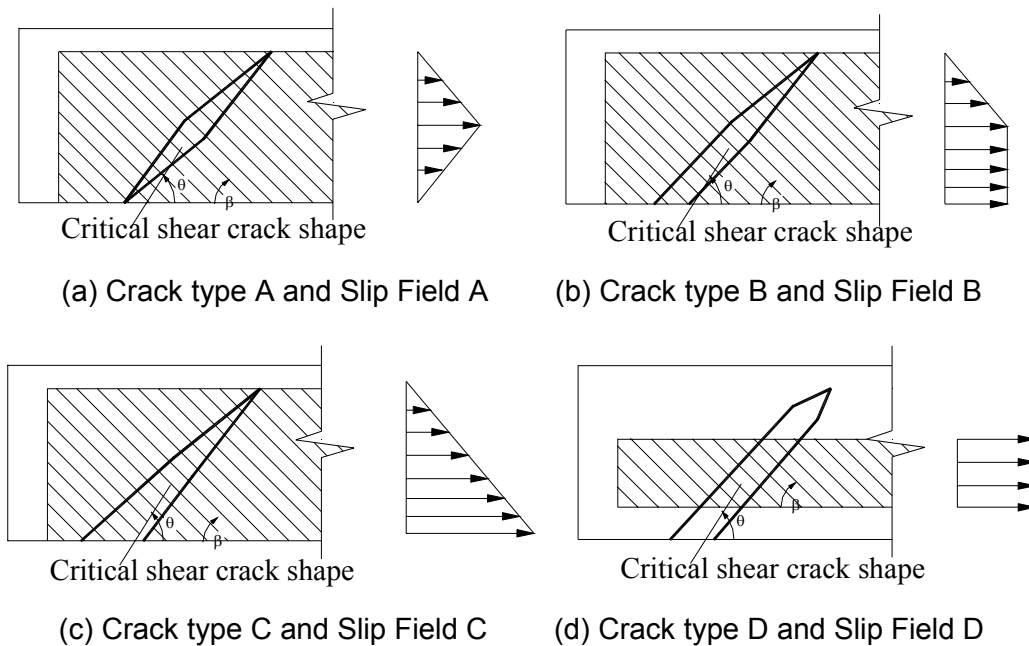


Figure 1 - Typical idealised crack shapes and slip fields

4. COMPUTATIONAL MODELS

For U-jacketed beams considered in this study, the FRP strips intersected by the critical shear crack usually debond from the concrete in the area above the crack as shown in Fig. 2. The critical area of FRP is marked as “effective FRP” in Fig. 2. In the following finite element analysis, only the bond resistance of this critical FRP area is considered. Based on the assumption that the interfacial slips on the two sides of the critical shear crack are symmetrical, the interfacial slip of the FRP in the critical area above the crack equals to half of the width of the critical shear crack. As a result, four simplified computational models (Fig. 2) can be established, corresponding to the four types of cracks (Fig. 1). It may be noted that the assumption that the slip is symmetrical on the two sides of the crack is not exactly valid, but numerical results from more complete models considering the full height of the FRP intersected by the crack show that the error resulting from this simplistic treatment is insignificant.

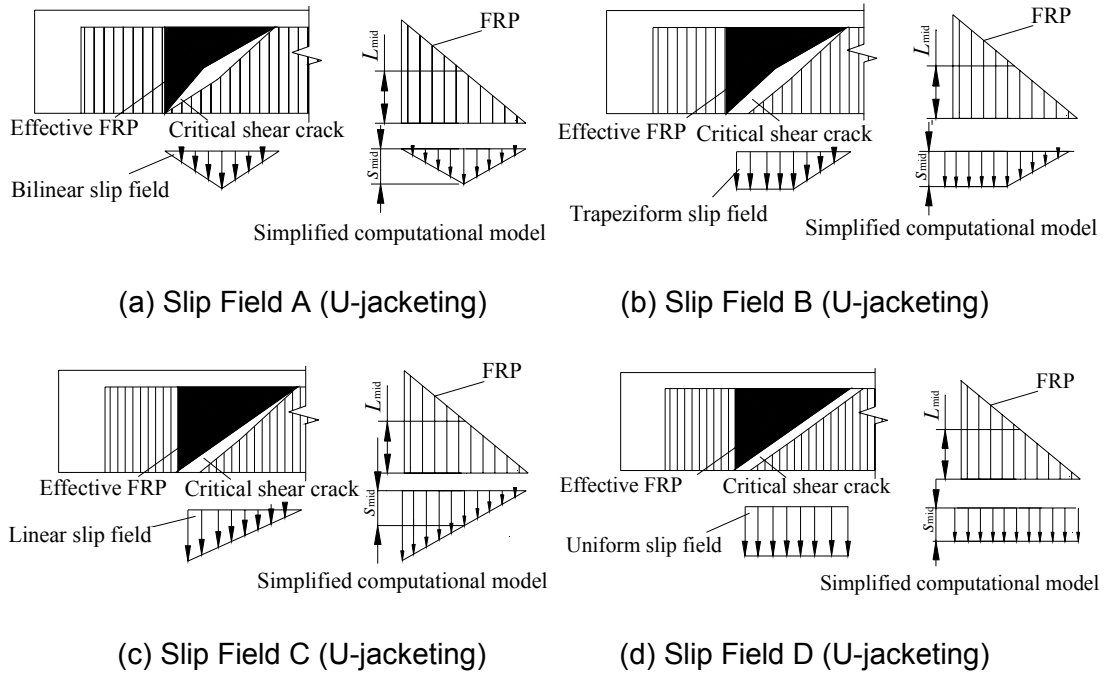


Figure 2 - Computational models

5. FINITE ELEMENT IMPLEMENTATION

The idealised computational models shown in Fig. 2 were implemented using ANSYS [20]. The FRP strips were modelled by a series of truss elements, whilst the interfaces were modelled by a series of spring elements, as shown in Fig. 3. The truss elements were connected to the rigid substrate concrete (e.g. deformations of un-cracked concrete were ignored) using the spring elements. The bond-slip relationship proposed by Lu et al. [17] (Fig. 4) was used to derive the properties of the spring elements. The LINK 1 element in ANSYS was used to model the FRP truss elements and the COMBIN 39 element was used to model the spring elements.

The loading process was effected by continuously increasing the displacements of the truss elements at the boundary that represents the critical shear crack, according to one of the four different slip fields (Fig. 2). An analysis was terminated when the average stress in the FRP $\sigma_{f,ave}$ was reduced to half of its peak value. The results were then used to deduce the average FRP stress and the FRP stress distribution factor at different slip values.

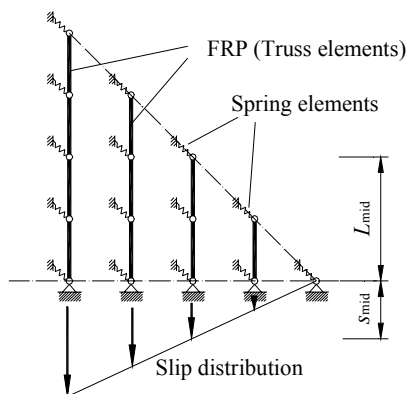


Figure 3 - Finite element models (Slip Field C)

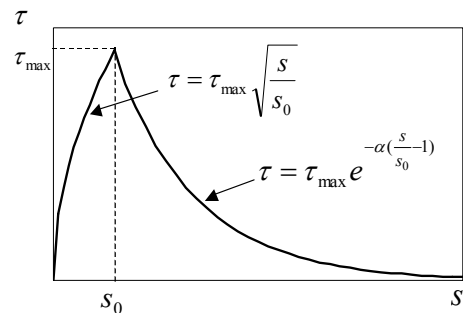


Figure 4 - Bond-slip model [17]

6. NUMERICAL RESULTS

6.1 Development of stresses in FRP

Figure 5 shows a typical example of the variation of the average FRP stress against the increase of slip at the mid-height of the effective FRP for a U jacked beam for different slip fields. Here the average FRP stress $\sigma_{f,ave}$ is normalised by $\sigma_{f,inf}$, and the slip at the mid-height s_{mid} is normalised by the slip at the peak interfacial stress s_0 (Fig. 4). The following parameters were used in this example: concrete tensile strength $f_t = 3\text{MPa}$, axial stiffness of FRP $E_f t_f = 16\text{GPa}\cdot\text{mm}$, FRP strip width to spacing ratio $w_f/s_f = 0.5$, normalised FRP bond length at the mid-length of the crack (or mid-crack) $\lambda' = 1.5$.

Except for Model D, the FRP average stress reaches its peak value when the normalised slip at mid-height is about 7.5 (corresponding to a maximum crack width of about 0.88mm for Models A and B but 1.75mm for Model C). $\sigma_{f,ave}$ reduces rapidly after its peak value. For Slip Field D (uniform crack width), the behaviour is quite different, where $\sigma_{f,ave}$ reaches its peak value when s_{mid}/s_0 is only slightly greater than 1 (corresponding to a maximum crack width of about 0.12mm) but its descending rate thereafter is much smaller than other models. This is because the FRP strips in this model debond from the concrete one by one at a regular and slow pace. In Model C, the FRP strips debond from the concrete almost simultaneously because the variation of the bond length in the critical FRP area matches the distribution of the slip field. In general, a model that leads to a higher peak FRP average stress has a steeper descending branch, and predicts a failure process that is less ductile. It is interesting to note that the differences between the peak FRP average stresses from the four models are not large.

The distributions of the FRP stress over the height from the four models with $\lambda'=1.5$ are shown in Fig. 6 at their corresponding peaks of the FRP average stress. The distribution predicted by Chen and Teng's model [1, 2] is also shown for comparison. It is seen that Chen and Teng's prediction is in very close agreement with those from Slip Fields B and C. In Model D, the peak average stress is reached before the stress in any of the FRP strips reaches $\sigma_{f,inf}$ because the strips near the crack tip (top) start to debond from the concrete at a very early stage. For Model A, the stresses in the FRP strips close to the beam bottom are not well developed because the crack widens fastest at the mid-height of the beam.

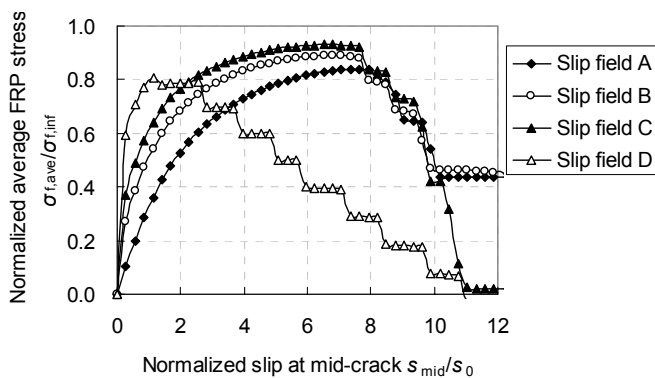


Figure 5 – Variation of average FRP stress with slip

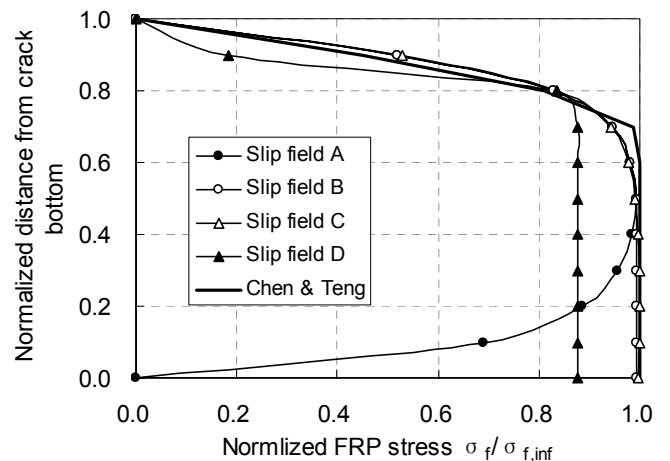


Figure 6 - FRP stress distribution at peak average stress ($\lambda'=1.5$)

6.2 Effect of beam size on FRP stress distribution

If the bonded FRP strips cover the full height of the beam on both sides, the normalised FRP bond length λ' is proportional to the beam height. Therefore, the effect of the beam size on the FRP stress distribution can be investigated by varying the normalised FRP bond length λ' . For different

λ' values, Fig. 7 shows the FRP stress distributions corresponding to the peak values of the FRP average stress for Model C. The FRP stress distribution is close to the shape of the slip field (linear in Model C) when λ' is very small because the slip is the largest at the bottom where the FRP bond length is also the largest. As the normalised bond length increases, the maximum FRP stress also increases until the maximum bond length (at the bottom of the crack) reaches the effective bond length. After that, the stress distribution in the FRP becomes more and more uniform because the FRP stress cannot exceed $\sigma_{f,inf}$.

6.3 Relationship between D_{fl} and λ'

As is evident from Eq. 7, the effective FRP stress can be easily obtained if the modified FRP stress factor D_{fl} is given. Furthermore, the FRP contribution to the shear capacity is proportional to D_{fl} . The effect of the bond length (beam size) on D_{fl} is investigated here for the four slip fields (Fig. 8). Chen and Teng's [1, 2] prediction is also shown for comparison. Although the four crack shapes are significantly different and they may represent some extreme scenarios, the predicted FRP stress factors are not significantly different. The maximum difference between the four models for $\lambda'=1$ is less than 15% and this difference reduces further as λ' increases. It is shown that Chen and Teng's prediction lies nicely between these four curves: it is generally higher than those from Models A and D, lower than that from Model C, and very close to but slightly lower than that from Model B. As noted earlier, the shape of the critical shear crack for most practical beams is expected to lie between those of Models A and C, which may explain the close agreement between Chen and Teng's shear strength model and independent test data [2]. Therefore, it may be concluded Chen and Teng's model is safe and accurate.

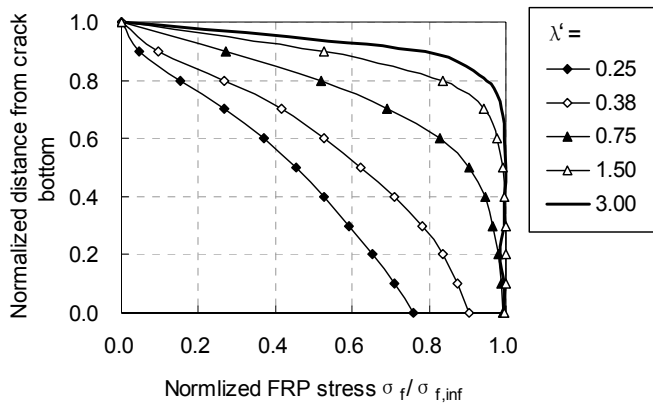


Figure 7 – FRP stress distributions at peak average stress (Slip Field C)

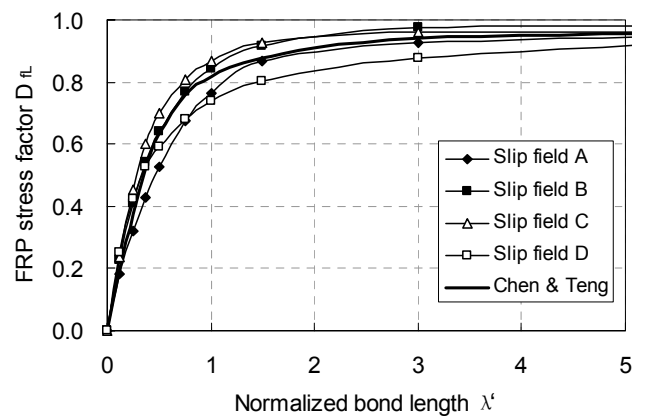


Figure 8 - $D_{fl} \sim \lambda'$ relationships from different models

7. CONCLUSIONS

This paper has presented a theoretical study on the stress distribution in the FRP in RC beams shear-strengthened with FRP U jackets at debonding failure. Four different idealised crack shapes for the critical shear crack were considered. A rigorous FRP-to-concrete bond-slip model was used to represent the interfacial behaviour between the FRP and the substrate concrete. The finite element method was employed to model the behaviour of an idealised system consisting of FRP strips bonded to a rigid concrete prism. Although the different crack shapes result in significantly different stress distributions in the FRP, their effect on the stress distribution factor is much less significant. The study confirms that Chen and Teng's [1, 2] simple assumption for the stress distribution in the FRP results in satisfactory predictions of the contribution of the FRP to the shear capacity of the beam.

8. ACKNOWLEDGEMENTS

The authors would like to acknowledge financial support provided by the Royal Society through Royal Society-NSFC UK-China Joint Project (Grant No. IS 16657), the Research Grants Council of the Hong Kong Special Administrative Region, China (Project No: PolyU 5151/03E), and the National Natural Science Foundation of China through a key project for FRP in construction (Project No. 50238030).

9. REFERENCES

1. Chen, J.F. and Teng, J.G. (2001). "Shear strengthening of RC beams by external bonding of FRP composites: a new model for FRP debonding failure", *Proc. (CD-ROM), 9th International Conference on Structural Faults and Repair*, 4-6 July, London.
2. Chen, J. F. and Teng, J. G. (2003). "Shear capacity of FRP-strengthened RC beams: FRP debonding", *Construction and Building Materials*, 17, 27-41.
3. ACI (2002). *Guide for the design and construction of externally bonded FRP systems for strengthening concrete structures*, ACI 440.2R-02, American Concrete Institute.
4. ISIS (2001). *Retrofitting concrete structures with fiber reinforced polymers*. ISIS Canada.
5. Chaallal, O., Nolle, M. J. and Perraton, D. (1998). "Strengthening of reinforced concrete beams with externally bonded fiber-reinforced-plastic plates: design guidelines for shear and flexure", *Canadian Journal of Civil Engineering*, 25(4), 692-704.
6. Concrete Society (2004). *Design guidance for strengthening concrete structures using fibre composite materials*, Technical Report No. 55, 2nd Edition, UK.
7. fib (2001). *Externally bonded FRP reinforcement for RC structures*, Task Group 9.3, International Federation for Structural Concrete (fib).
8. JSCE (2000). *Recommendations for upgrading of concrete structures with use of continuous fiber sheets*, Research Committee on Upgrading of Concrete Structures with Use of Continuous Fiber Sheets, Japanese Society of Civil Engineers.
9. Khalifa, A., Gold, W. J., Nanni, A. and Aziz, A. (1998). "Contribution of externally bonded FRP to shear capacity of RC flexural members", *Journal of Composites for Construction*, ASCE, 2(4), 195-203.
10. Maeda, T., Asano, Y., Sato, Y., Ueda, T. and Kakuta, Y. (1998). "A study on bond mechanism of carbon fiber sheet", *Proc., 3rd International Symposium on Non-Metallic (FRP) Reinforcement for Concrete Structures*, Sapporo, 279-285.
11. Triantafillou, T. C. (1998). "Shear strengthening of reinforced concrete beams using epoxy-bonded FRP composites", *ACI Structural Journal*, 95(2), 107-115.
12. Taljsten, B. (2003). "Strengthening concrete beams for shear with CFRP sheets", *Construction and Building Materials*, 17(1), 15-26.
13. Teng, J. G., Chen, J. F., Smith, S. T. and Lam, L. (2002). *FRP-strengthened RC structures*, John Wiley & Sons, UK.
14. Teng, J.G., Chen, J.F., Smith, S.T. and Lam, L. (2003). "Behaviour and strength of FRP-strengthened RC structures: a state-of-the-art review", *Proceedings of the Institution of Civil Engineers – Structures and Buildings*, 156(SB1), 51-62.
15. Chen, J.F. and Teng, J.G. (2001). "A shear strength model for FRP strengthened RC beams", *Proc., 5th International Conference on Fibre-Reinforced Plastics for Reinforced Concrete Structures (FRPRCS-5)*, Cambridge, 16-18 July, pp. 205-214.
16. Chen, J.F. and Teng, J.G. (2003). "Shear capacity of FRP strengthened RC beams: fibre reinforced polymer rupture", *Journal of Structural Engineering*, ASCE, 129(5), 615-625.
17. Lu, X. Z., Teng, J. G., Ye, L. P. and Jiang, J. J. (2005). "Bond-slip models for FRP sheets/plates externally bonded to concrete", *Engineering Structures*, 27(6), 938-950.
18. Chen, J. F. and Teng, J. G. (2001). "Anchorage strength models for FRP and steel plates bonded to concrete", *Journal of Structural Engineering*, ASCE, 127(7), 784-791.
19. Teng, J. G., Yuan, H. and Chen, J. F. (2005). "Theoretical model of FRP-to-concrete interfaces between two adjacent cracks", to be published.

20. ANSYS. (1999). *User's Manual*, ANSYS Company.